AGU PUBLICATIONS

JGR

Journal of Geophysical Research: Atmospheres

RESEARCH ARTICLE

10.1002/2014JD021686

Key Points:

- Snow particle speeds in drifting snow were obtained
- Snow particle speed was always less than wind speed below a height of 1 m
- Dependence of particle speeds on both grain size and wind speed were revealed

Correspondence to:
K. Nishimura,
knshi@nagoya-u.jp

Citation:
Nishimura, K., C. Yokoyama, Y. Ito, M. Nemoto, F. Naaim-Bouvet, H. Bellot, and K. Fujita (2014), Snow particle speeds in drifting snow, *J. Geophys. Res. Atmos.*, *119*, 9901–9913, doi:10.1002/2014JD021686.

Received 24 FEB 2014
Accepted 2 AUG 2014
Accepted article online 7 AUG 2014
Published online 25 AUG 2014

Snow particle speeds in drifting snow

Kouichi Nishimura[1], Chika Yokoyama[1], Yoichi Ito[1,3], Masaki Nemoto[2], Florence Naaim-Bouvet[3,4], Hervé Bellot[3,4], and Koji Fujita[1]

[1]Graduate School of Environmental Studies, Nagoya University, Nagoya, Japan, [2]Snow and Ice Research Center, NIED, Nagaoka, Japan, [3]Irstea, UR ETNA, Saint-Martin d'Hères, France, [4]University Grenoble Alpes, Grenoble, France

Abstract Knowledge of snow particle speeds is necessary for deepening our understanding of the internal structures of drifting snow. In this study, we utilized a snow particle counter (SPC) developed to observe snow particle size distributions and snow mass flux. Using high-frequency signals from the SPC transducer, we obtained the sizes of individual particles and their durations in the sampling area. Measurements were first conducted in the field, with more precise measurements being obtained in a boundary layer established in a cold wind tunnel. The obtained results were compared with the results of a numerical analysis. Data on snow particle speeds, vertical velocity profiles, and their dependence on wind speed obtained in the field and in the wind tunnel experiments were in good agreement: both snow particle speed and wind speed increased with height, and the former was always 1 to 2 m s^{-1} less than the latter below a height of 1 m. Thus, we succeeded in obtaining snow particle speeds in drifting snow, as well as revealing the dependence of particle speed on both grain size and wind speed. The results were verified by similar trends observed using random flight simulations. However, the difference between the particle speed and the wind speed in the simulations was much greater than that observed under real conditions. Snow transport by wind is an aeolian process. Thus, the findings presented here should be also applicable to other geophysical processes relating to the aeolian transport of particles, such as blown sand and soil.

1. Introduction

Drifting snow is a leading agent in the dynamics of numerous climatic and hazardous processes. The redistribution of snow by wind is important for hydrological and mass balance processes, especially in Arctic and Antarctic regions. In mountainous regions, locally increased snow drifts and snow cornices caused by drifting snow lead to avalanche release. Furthermore, on roads, drifting snow causes snowdrifts and reduces visibility. Thus, drifting snow has been the subject of previous studies [e.g., *Armstrong and Brun*, 2010; *Nemoto and Nishimura*, 2004]. However, our understanding of the internal structures of drifting snow is still far from satisfactory.

Snow transport by wind is an aeolian process. *Bagnold* [1941] identified three modes of aeolian sand transport: saltation, suspension, and surface creep. Generally, once the wind speed over a grain surface is sufficient for entrainment in the air stream, the grains move along parabolic trajectories in a process called "saltation," then, the grains are accelerated by the drag of the wind, collide with other particles, and return to the bed with increased momentum. At higher wind speeds, the particles are transported upward by turbulent eddies and are thus transported far downwind of their original bed location; this is the process of "suspension." Although Bagnold used "surface creep" to describe grains rolling and jostling along the bed surface, surface creep has been redefined and renamed "reptation," which describes grains making short hops just above the surface, having been ejected by a saltating particle [*Unger and Haff*, 1987]. The physical processes of aeolian particle transport are described in detail by *Anderson et al*. [1991]. Numerous attempts have been made to understand the processes of sand transport by wind. Mass flux and wind speed profiles have been measured in wind tunnels and in the field [e.g., *Anderson and Haff*, 1991; *Rasmussen and Mikkelsen*, 1998; *White and Mounla*, 1991]. Numerical simulations have also been conducted, for instance by *McEwan and Willetts* [1991] and *Shao and Li* [1999], based on modeling of four fundamental subprocesses of aeolian transport: aerodynamic entrainment, grain trajectories, grain-bed collisions, and wind modification. A self-regulating system of saltation [*Anderson and Haff*, 1991] was well demonstrated using these models. Furthermore, attempts have been made to model sand transport under the influence of turbulence. *Tong and Huang* [2012] obtained wind velocities by solving for the flow field using a large eddy simulation approach, and a discrete element method was used to obtain the velocities and positions of moving particles.

Numerical drifting snow models, field observations, and wind tunnel experiments are all useful for the investigation of drifting snow phenomena. However, improvements in the techniques for investigating drifting snow are essential at this early stage of our understanding of this complex phenomenon. For instance, in the turbulent diffusion model of drifting snow [e.g., *Bintanja*, 2001; *Dery and Yau*, 1999; *Gauer*, 1998; *Naaim et al*., 1998; *Uematsu*, 1993], it is usually assumed that air and snow particles behave in the same manner; the Schmidt number, which is the ratio between the diffusion coefficients of air and snow particles, is assumed to have a value of 1, and particle fall speeds are assumed to fit observed concentrations. On the other hand, in the Lagrangian model of drifting snow [e.g., *Doorschot and Lehning*, 2002; *Nemoto and Nishimura*, 2004], which describes individual particle motions, several assumptions and arbitrary parameters are invoked. For instance, splash processes at higher friction velocities need to be understood. If bed grains are fully fluidized under a strong wind, splash processes on the bed will likely differ significantly from those under weaker winds. Furthermore, the aerodynamic entrainment of particles from the surface should be defined in conjunction with the turbulent structure. Regardless, particle speeds in drifting snow are a key issue in both the turbulent diffusion and random flight models of drifting snow, and thus, direct measurements of particle speeds are needed.

In addition to computer simulations, wind tunnel experiments have been conducted to observe the behavior of saltating particles. *Nishimura and Hunt* [2000] analyzed the trajectories of particles, recorded using a stroboscopic light and a high-speed video system, to examine differences between the speeds of ascending and descending particles. However, particle concentrations tend to increase with increasing friction velocity u_*, and therefore, distinguishing between individual particles at high particle concentrations was difficult. Thus, the particle speed was difficult to obtain except around the threshold friction speed u_*, where both wind speeds and particle concentrations are low. In addition, it was possible to detect the motions of only the larger particles, and thus, particle size dependencies were not accounted for. *Willetts and Rice* [1985], *Nalpanis et al*. [1993], and *Araoka and Maeno* [1981] also faced the same difficulties in their wind tunnel research of sand and snow transport.

Recently, leading edge technologies such as those of laser Doppler anemometry, particle image velocimetry, and particle-tracking velocimetry have been applied to the measurement of sand particle speeds in the saltation layer [*Creyssels et al*., 2009; *Liu and Dong*, 2004; *Rasmussen and Sorensen*, 2005; *Yang et al*., 2007]. These studies showed that particle concentration decreased exponentially with increasing height above the bed and in contrast to the logarithmic profile of the wind. Particle velocity varied linearly with height. However, because of the large concentration near the bed, it was difficult to make reliable measurements. Therefore, the dependency of particle speed on particle size remains difficult to measure. Furthermore, measurements have been limited to those obtained at wind tunnel scales, and no measurements have yet been conducted in the field.

In this study, we used a snow particle counter (SPC), which measures the accumulated snow particle size distribution and the mass flux at 1 s intervals [*Sato et al*., 1993]. We directly recorded the raw high-frequency signal from the SPC transducer and measured particle sizes and durations of passages of individual particles through the sampling area, and on this basis, we calculated particle speeds.

Experiments were first conducted using three SPCs at Col du Lac Blanc in the French Alps in March 2012. More precise measurements were then obtained in the cold wind tunnel at the National Research Institute for Earth Science and Disaster Prevention (NIED), Japan, which is 15 m long and has a working cross-sectional area of 1 × 1 m. The results of the field and wind tunnel experiments were then compared with calculations of a random flight simulation [*Nemoto and Nishimura*, 2004]. The model uses Lagrangian stochastic theory to account for turbulence effects on the suspension of snow grains and also includes aerodynamic entrainment, grain-bed collision processes, wind modification by grains, and the distribution of grain sizes.

2. Instruments and Methods

2.1. SPC

The SPC used in this study (Niigata Denki Co.) (Figure 1) is an optical device [*Nishimura and Nemoto*, 2005] that measures the diameter and the number of drifting snow particles by detecting their shadows on a photodiode (assuming that drifting particles are spherical in shape). In contrast to the SPC originally

Figure 1. Snow particle counter (SPC).

developed by *Schmidt* [1977], the SPC used here is a single slit sensor with a laser diode, which produces a more strongly collimated light beam. Electric pulse signals resulting from snow particles passing through the sampling volume (2 mm × 25 mm × 0.5 mm) are sent to a transducer and an analyzing data logging system (PC). In this way, the SPC is able to detect particles in the range of 40–500 μm. The analysis software divides the particles into 32 size classes and records the number of particles in each size class at 1 s intervals. The SPC is mounted on a self-steering wind vane, and hence, the sampling region, which has a cross-sectional area of 2 mm × 25 mm (50 mm^2), is maintained perpendicular to the horizontal wind vector. If the diameter of a snow particle is larger than that of the maximum diameter class, the snow particle is considered to belong to the maximum diameter class. Usually, SPCs are used to observe the snow particle size distribution and mass flux at 1 s intervals. However, in this study, the output signal from the transducer was directly recorded at a frequency of 150 kHz for the field measurements and 100 kHz for the wind tunnel experiments (see the wave form in Figure 2), yielding much higher resolution data than obtained using digital data recorded at 1 s intervals. Thus, the peak of the SPC output, which corresponds to particle size *d* and duration *t* over which the particle passes through the sampling area, allows calculation of the particle speed *v* according to

$$v = \frac{L + d}{t} \tag{1}$$

where *L* is the length of the sampling area in the direction of wind flow (500 μm).

2.2. Field Measurements

Measurements were first conducted at Col du Lac Blanc in the French Alps, a large north–south-oriented pass located near Alpe d'Huez ski resort at an elevation of 2720 m above sea level. The terrain on the pass is relatively flat over a distance of approximately 300 m. Moreover, drifting snow has been studied at this location for 20 years by the Institut National de Recherche en Sciences et Technologies pour l'Environnement et l'Agriculture IRSTEA (formerly the Centre National du Machinisme Agricole, du Génie Rural, des Eaux et des Forêts; CEMAGREF) and Meteo France. As a result of the surrounding topography, 90% of the observed winds blow from the northeast and south. Three SPCs were installed on a mast (Figure 3). One SPC was mounted in a fixed orientation at a height *z* of 3.42 m above the snow surface. The other two were mounted near the snow pack surface (0.02 m and 1.04 m above the snow surface or 0.31 m and 1.33 m above the snow surface), and their orientations were adjusted manually. Output signals from the SPCs were transmitted and recorded at 150 kHz for periods lasting 100 s. Two cup

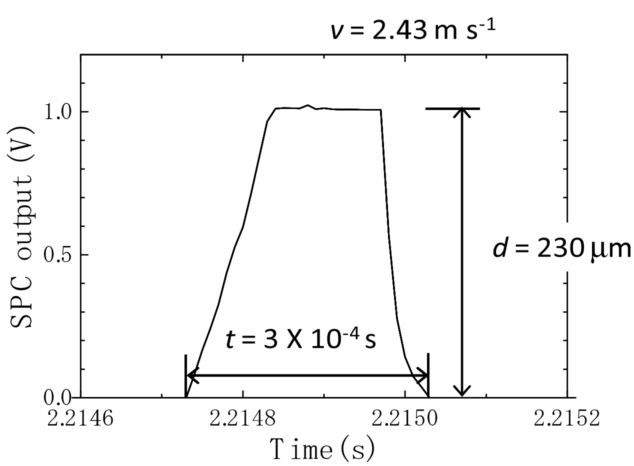

Figure 2. Waveform from the snow particle counter (SPC), recording the passage of a snow particle.

Figure 3. Experimental setup at Col du Lac Blanc.

anemometers (AF860, Makino Applied Instruments Inc.) were mounted at 1.37 m and 0.35 m above the snow surface. In addition, an ultrasonic anemometer (USA-1, Metek) was mounted at $z = 2.17$ m above the snow surface. Measurements were conducted during 1330–1530 LT on 5 March 2012. Air temperature, wind speed, wind direction, and snow depth during the observation period were −16°C, 5 to 11 m s^{-1} at a height of 2.17 m, northeast, and 1.1 m around the mast, respectively. A 2 to 3 cm thick layer of "Decomposing and Fragmented Precipitation Particles" layer was present on the compacted "Rounded Grains" snow [*Fierz et al*., 2009].

2.3. Wind Tunnel Experiments

Experiments were conducted in a cold wind tunnel at the Cryospheric Environmental Simulator (CES) of the National Research Institute for Earth Science and Disaster Prevention (NIED), Japan (Figure 4). The tunnel, which is based on a return-flow closed-circuit design, is 15 m long, 1 m wide, and 1 m high. Spires were used to generate large-scale vortices at the windward end of the working section, which created a steady uniform logarithmic boundary layer approximately 0.2 m deep. Compacted snow sieved through 0.5–1.0 mm mesh was placed on the wind tunnel floor to a depth of approximately 20 mm, to reproduce the conditions of the field measurements at Col du Lac Blanc as closely as possible.

The snow surface was smoothly prepared by hand using a steel rake. The air temperature was set to −15°C. To initiate and maintain steady saltation, seed particles were supplied at a constant rate at the bottom of the entrance to the wind tunnel. Further details of the wind tunnel are described in *Sato et al*. [2001]. Wind speeds were measured using a microultrasonic anemometer (TR-92 T, Kaijo Co.); this anemometer has a small probe span (30 mm) and can measure wind speeds with a time resolution of 20 Hz. The SPC and an ultrasonic anemometer were set 0.2 m apart at the same height above the snow surface (Figure 4). Measurements were taken at free stream velocities of 8 m s^{-1}, 10 m s^{-1}, and 12 m s^{-1} in the wind tunnel and at the level of the sensors (0.015–0.15 m above the snow surface). Measurements were taken at points 12 m or 6 m leeward of the wind tunnel entrance.

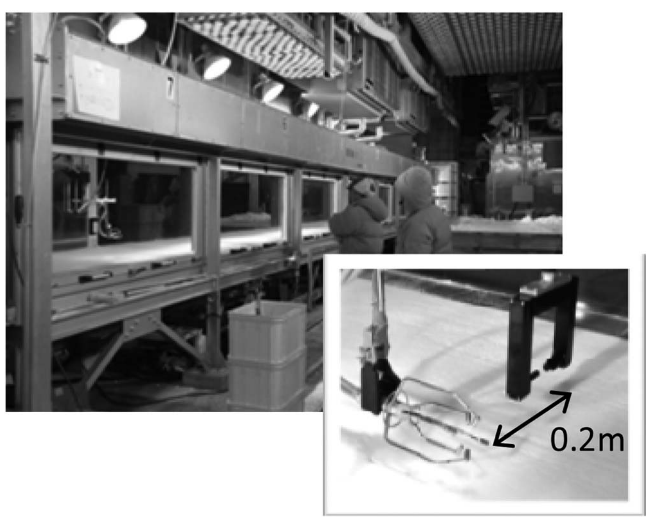

Figure 4. Cold wind tunnel at the Cryospheric Environmental Simulator (CES), National Research Institute for Earth Science and Disaster Prevention (NIED), Japan.

Figure 5 shows an example how the mass flux at a height of 3 cm changed during an experiment when wind speeds were 8 m s^{-1}. The seeding of snow particles, which started at 23 s, initiated the drifting of snow, and the mass flux increased rapidly. Then, during 40–100 s, the average of the mass flux was kept nearly constant. Sampling was performed for 60 s at each level, and the analyses were performed on 10 s intervals of data. *Okaze et al*. [2012] confirmed that even

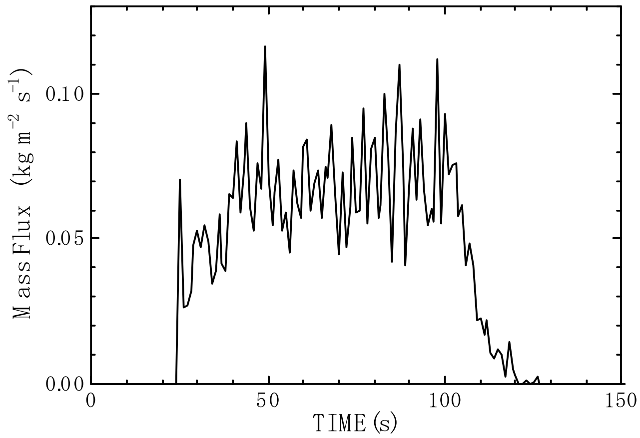

Figure 5. Snow mass flux change in the wind tunnel. Measurements were conducted at a height of 3 cm in a free stream velocity of 8 m s^{-1} ($u_* = 0.37$ m s^{-1}).

6 s is a sufficient time to obtain stable statistical values.

2.4. Random Flight Model of Blowing Snow

Nemoto and Nishimura [2004] proposed a numerical drifting snow model that incorporates turbulent flow, using Lagrangian stochastic theory to simultaneously model saltation and suspension modes. The model takes all physical processes into consideration including aerodynamic entrainment, grain-bed collisions, wind speed modifications, particle size distributions, and turbulent fluctuations, and their effects on particle trajectories. The mean horizontal wind velocity U is given as

$$\frac{dU}{dt} = \frac{1}{\rho_a}\frac{d}{dz}\left(\rho_a \kappa^2 z^2 \frac{dU}{dz}\frac{dU}{dz}\right) + \frac{1}{\rho_a}\sum_{i=1}^{n} m_i \left(\frac{dv_x(z)}{dt}\right)_i, \tag{2}$$

where ρ_a is the density of the air and κ is von Karman's constant (= 0.4). The second term on the right-hand side of the equation is the force per unit volume exerted on the fluid by the grains acting in the direction of flow, n is the number of grains per unit volume of fluid at height z, m_i is the mass of grain i, and $\left(\frac{dv_x(z)}{dt}\right)_i$ is the horizontal acceleration of grain i at height z.

The Lagrangian stochastic (random flight) model, which describes the paths of particles in a turbulent flow, has been applied to the description of many atmospheric diffusion processes (e.g., those involving pollen and air pollutants) and has been used to describe turbulence [*Wilson and Sawford*, 1996]. Very close to

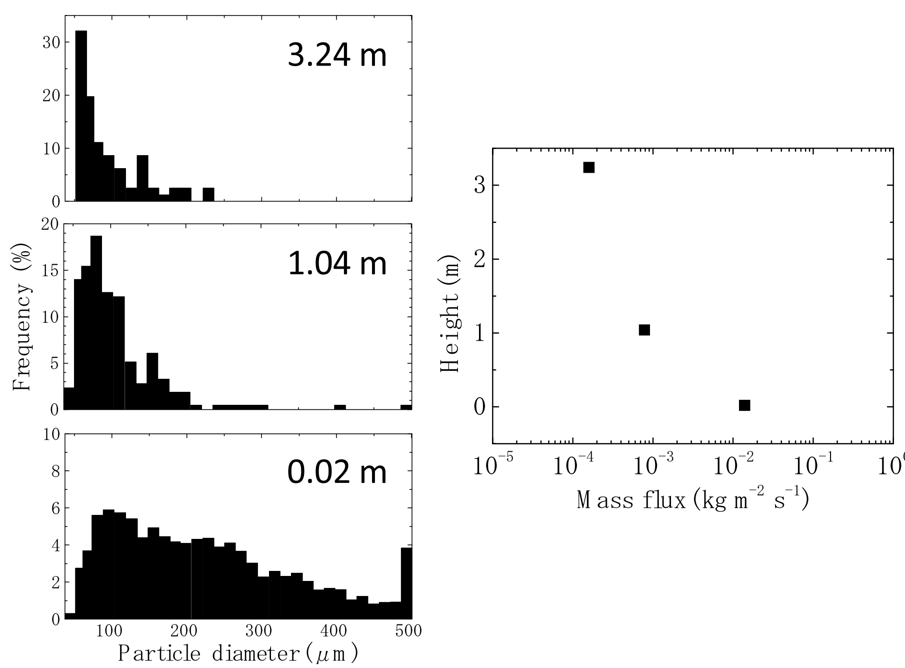

Figure 6. Snow particle diameter distributions and horizontal mass flux values determined for case A.

10.1002/2014JD021686

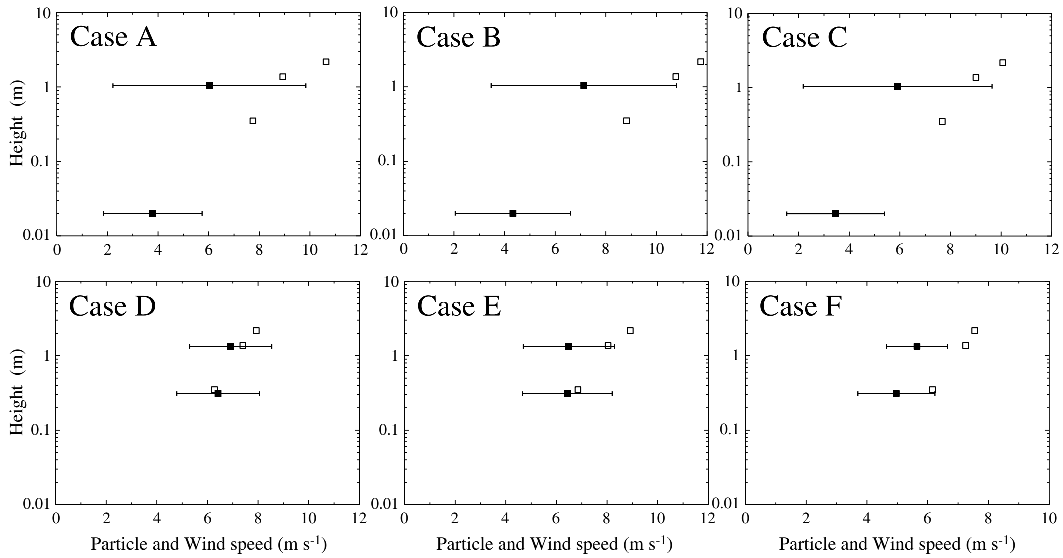

Figure 7. Snow particle speed (black square, mean; bar, one standard deviations on either side of the mean) and wind speed (white square, mean) distributions in drifting snow conditions.

the ground, the mean velocity is sufficiently large in comparison with typical velocity fluctuations that only vertical fluctuations w' need to be considered. For a blowing snow particle i, w' is expressed as

$$w_i^{'} = \left(1 - \frac{\Delta t}{T_l}\right) w_{i-1}^{'} + \sigma_w \sqrt{\frac{2}{T_l} W_t}, \tag{3}$$

where σ_w is the standard deviation of the vertical fluctuations, W_t is a Gaussian random variable with a mean of zero and unit variance, and T_l is the Lagrangian time scale. It is important to note that heavy particles do not follow fluid element motion exactly. Thus, two additional effects must be considered. First, heavy particles have fall velocities due to the gravitational force, which affects the fluctuations in the fluid velocities sampled by the heavy particles. Second, particle inertia prevents heavy particles from following the fluctuations of the turbulence. These two effects bring about a "crossing trajectories" effect (the particle cuts across the trajectories of fluid elements). *Hunt and Nalpanis* [1985] modeled the vertical fluid velocity of a particle using equation (3) but at a small time scale T_l*, according to

$$T_l^* = T_l 1 / \left(1 + A_1 \left(\frac{V_R}{\sigma_w}\right)^{2/3} \left(\frac{T_l}{\Delta t}\right)^{1/3}\right) \tag{4}$$

where V_R is the relative velocity (=$v - U$) and A_1 is a dimensionless constant of $O(1)$.

The motion of a spherical particle in wind can be described by the following equations [*Nishimura and Hunt*, 2000]:

$$\frac{dV_1}{dt} = -\frac{3}{4}\left(\frac{\rho_a}{\rho_p d}\right) C_D V_R V_{R1} \tag{5}$$

$$\frac{dV_3}{dt} = -\frac{3}{4}\left(\frac{\rho_a}{\rho_p d}\right) C_D V_R V_{R3} - g, \tag{6}$$

Table 1. Friction Velocities and Roughness Parameters in the Drifting Snow Measurements at Col du Lac Blanc in the French Alps at 1330 to 1530 LT on 5 March 2012

Case	A	B	C	D	E	F
Friction velocity: u_* (m/s)	0.35	0.57	0.32	0.35	0.43	0.31
Roughness length: z_0 (m)	4.5×10^{-5}	7.3×10^{-4}	3.2×10^{-6}	3.0×10^{-4}	6.3×10^{-4}	1.2×10^{-4}

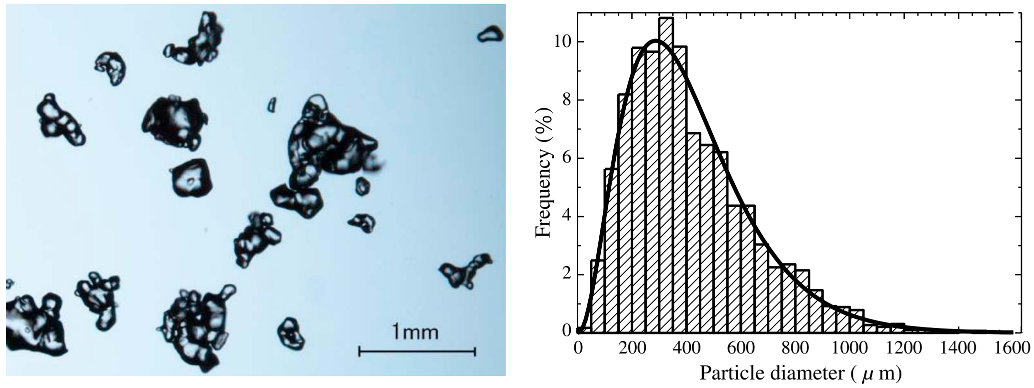

Figure 8. (left) Snow particles and (right) the particle diameter distribution used in the wind tunnel experiments.

where V_1 and V_3 are the horizontal and vertical components of the particle velocity, respectively, d is the particle diameter, ρ_p is the density of the particle, and g is the acceleration of gravity. The relative velocity between the wind and the particle V_R is given as

$$V_R = \left((V_1 - U)^2 + (V_3 - \omega')^2\right)^{1/2}. \tag{7}$$

The drag coefficient C_D for a spherical grain is a function of its Reynolds number. In the calculations, we used an empirical function given by *Morsi and Alexander* [1972] to determine C_D. The mean horizontal wind speed U was assumed to increase logarithmically with height, as is typical for the neutral atmospheric condition. A splash function that prescribes particle-bed collision processes was formulated on the basis of the experimental data of *Sugiura and Maeno* [2000]. The domain over which the particles move is 1 m in length streamwise, 0.01 m in width, and 20 m in height. To reduce the computational load, the streamwise direction was assigned periodic boundary conditions. The wind velocity was calculated every 10^{-2} s and each particle trajectory every 10^{-4} s. A detailed explanation of the blowing snow model and of the simulation procedure used in this study is given in *Nemoto* [2002] and *Nemoto and Nishimura* [2004].

In section 4, snow particle speeds obtained in both the field and the wind tunnel are compared with the numerical simulations.

3. Results

3.1. Field Measurements

Measurements were conducted at eight different times; in two cases, slight snowfall was present during sampling. To avoid the effects of snowfall on the analysis, we here introduce the six cases for which snow precipitation was absent at the time of sampling. As stated, data were recorded for 100 s during each run; however, notable changes in the wind speed were recorded during the measurement interval. Thus, the analyses were performed on 2–10 s intervals of data, during which wind speeds were nearly constant.

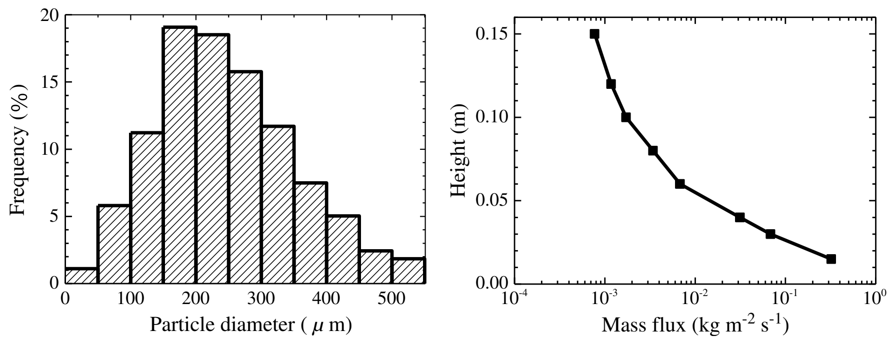

Figure 9. (left) Particle size distribution at 0.015 m high and (right) horizontal mass flux distribution at $u_* = 0.37$ m s^{-1}.

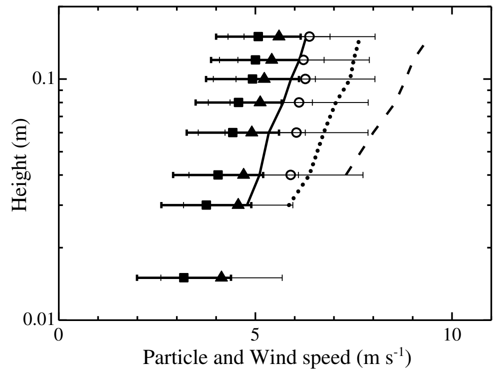

Figure 10. Particle and wind speed distributions for $u_* = 0.37\ \mathrm{m\,s^{-1}}$ (black square: particle speed; solid line: wind speed), $0.45\ \mathrm{m\,s^{-1}}$ (black triangle: particle; dotted line: wind speed), and $0.63\ \mathrm{m\,s^{-1}}$ (white circle: particle; broken line: wind speed) (data points represent mean values, and the bars represent one standard deviation on either side of the mean).

Hereafter, we refer to the six cases as cases A–F. Figure 6 shows examples of snow particle diameter distributions and the horizontal mass flux measured using the SPCs. For case A, the wind speed at a height of 2.17 m was approximately $10\ \mathrm{m\,s^{-1}}$, and particle diameters were widely distributed over the range of 50–500 μm. However, the proportion of small particles increased with increasing height, particularly for particles with diameters of <100 μm. The horizontal mass flux showed an exponential decay with height, a result which is similar to that obtained by a number of researchers [*Greeley et al.*, 1996; *Kind*, 1992; *Nishimura and Nemoto*, 2005; *Takeuchi*, 1980].

Snow particle speeds obtained with the high-frequency sampling of the SPC are shown as a function of height in Figure 7, along with wind speeds measured with the ultrasonic anemometer and the cup anemometers. Friction velocities and roughness parameters obtained for the individual cases using the wind speed profiles are listed in Table 1. In all cases, wind speeds and particle speeds increased monotonically with height, although fluctuations in the cup anemometer data are fairly large. Generally, the wind speed was higher than the particle speed at each measuring point. The ratio between particle speed at a height of 1.33 m and wind speed at a height of 1.37 m was 0.78 to 0.93 and between particle speed at a height of 0.31 m and wind speed at a height of 0.35 m was 0.81 to 0.98 (cases D to F in Figure 7). It should be noted that differences between wind and particle speeds appear to decrease with decreasing height, which suggests that the speeds are close to one another near the snow surface; in fact, in case D, the particle speed is actually slightly higher than the wind speed at $z = 0.30$ m.

3.2. Wind Tunnel Experiments

Figure 8 shows images of representative snow particles and the diameter distribution of the 2929 samples used in the wind tunnel experiments. The latter can be accurately approximated by means of a two-parameter gamma probability density function [*Budd*, 1966; *Schmidt*, 1982], according to

$$f(d) = \frac{d^{\alpha-1}}{\beta^{\alpha}\Gamma(\alpha)} \exp\left(-\frac{d}{\beta}\right) \tag{8}$$

where d is the particle diameter, α is a shape parameter that determines the skewness of the distribution, and β is a shape parameter that describes the width/scale of the distribution. As the mean and variance of the distribution are $\alpha\beta$ and $\alpha\beta^2$, respectively, the parameters α and β can be easily evaluated. Here we determined values of $\alpha = 3.25$ and $\beta = 127.80$.

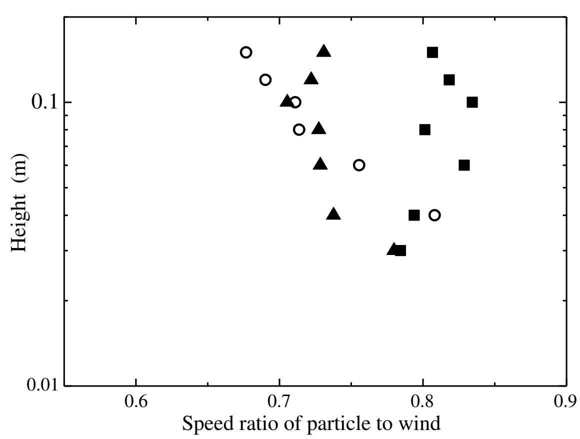

Figure 11. Ratio of particle speed to wind speed for $u_* = 0.37\ \mathrm{m\,s^{-1}}$ (black square), $0.45\ \mathrm{m\,s^{-1}}$ (black triangle), and $0.63\ \mathrm{m\,s^{-1}}$ (white circle) (data points represent mean values).

Figure 9 shows the particle size distribution at a height of 0.015 m and the horizontal mass flux distribution as a function of height, for wind speeds at the center of the wind tunnel of $8\ \mathrm{m\,s^{-1}}$. As shown by the field measurements (Figure 6), particle sizes near the snow surface (height of 0.015 m) are large, and the distribution becomes increasingly skewed with increasing height. However, overall, the mode of the particle size distribution decreases with increasing height. The horizontal mass flux shows an exponential decay with height, as was also

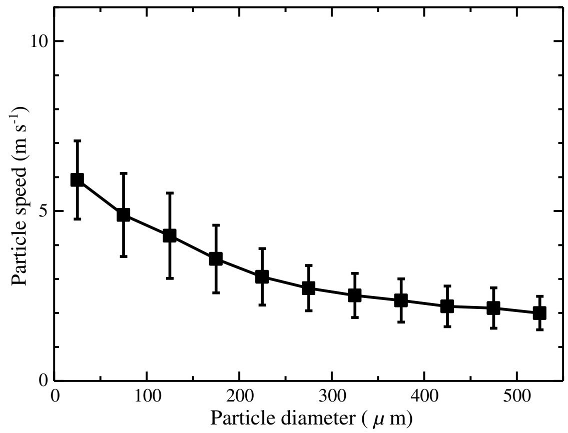

Figure 12. Snow particle speeds at $z = 0.015$ m as a function of diameter (at $u_* = 0.37$ m s^{-1}). Symbols represent mean values, and bars indicate one standard deviation on either side of the mean.

found in the field experiments (Figure 6). The same trends were observed in all of the experiments, regardless of wind speed and location in the wind tunnel.

Figure 10 shows particle speed and wind speed distributions measured with the SPC and the ultrasonic anemometer, respectively, for wind speeds at the center of the wind tunnel of 8, 10, and 12 m s^{-1}. These correspond to friction velocities u_* of 0.37, 0.45, and 0.63 m s^{-1} and roughness lengths z_0 of 1.82×10^{-5}, 1.45×10^{-5}, and 3.82×10^{-5} m, respectively. At $u_* = 0.37$ m s^{-1}, wind speeds increased from 4.8 to 6.2 m s^{-1} at heights of 0.03 to 0.15 m, and particle speeds also showed a monotonic increase with height (e.g., 3.2 m s^{-1} at 0.015 m versus 5 m s^{-1} at 0.1 m), although the range of the particle data is fairly large (nearly 2 m s^{-1}). The experiments show that particle speeds are less than wind speeds at all heights. Similar trends were recognized in two experiments, despite the fact that differences between wind and particle speeds increase at higher wind speeds. The ratios between particle speeds and wind speeds are shown in Figure 11. When u_* was 0.37 m s^{-1}, the ratios were 0.78 to 0.83 and they did not show any specific trend with height. However, at higher wind speeds, the height dependence became clearer, and the ratios at greater heights were smaller (0.78 to 0.72 at $u_* = 0.45$ m s^{-1} and 0.81 to 0.68 at $u_* = 0.63$ m s^{-1}). It should also be noted that the ratios were generally lower than those measured in the field experiments: 0.78 to 0.93 at height of 1.3 m and 081 to 0.98 at a height of 0.31 m.

Figure 12 gives an example of how particle speeds change with particle diameter, at $z = 0.015$ m and a wind velocity of 0.37 m s^{-1}. Mean particle speeds decreased from 6 m s^{-1} to 2 m s^{-1} with increasing particle diameter. Assuming that wind speeds maintain a trend similar to those shown in Figure 10 and can be extrapolated to lower heights, the wind speed at $z = 0.015$ m is approximately 4 m s^{-1}. Figure 12 indicates that the mean particle speed for particles of 100 μm is nearly 4 m s^{-1}. These observations allow us to estimate that a diameter of 100 μm is a critical diameter at a height of 0.015 m; particles smaller than 100 μm in diameter travel more quickly than the wind speed, whereas particles larger than 100 μm in diameter travel more slowly than the wind speed. As explained above, at higher wind speeds, particles are transported upward by turbulent eddies and by this means can be transported far downwind of their original bed location; this process is referred to as suspension. Particles in this mode obtain momentum from the wind and increase in speed. It should also be noted that particle sizes decrease with increasing height (Figure 6),

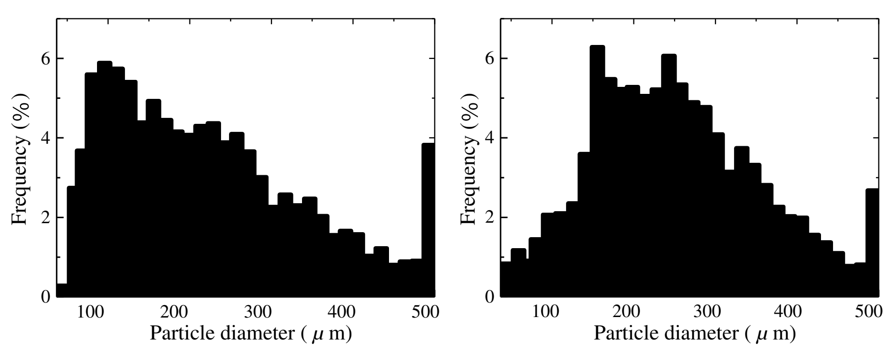

Figure 13. Particle diameter distributions. (left) Measured in the field at $z = 0.02$ m (case A); the friction velocity u_* was 0.35 m s^{-1}, and the roughness length z_0 was 4.5×10^{-5} m. (right) Measured in the wind tunnel at $z = 0.015$ m; u_* was 0.37 m s^{-1}, and z_0 was 1.82×10^{-5} m.

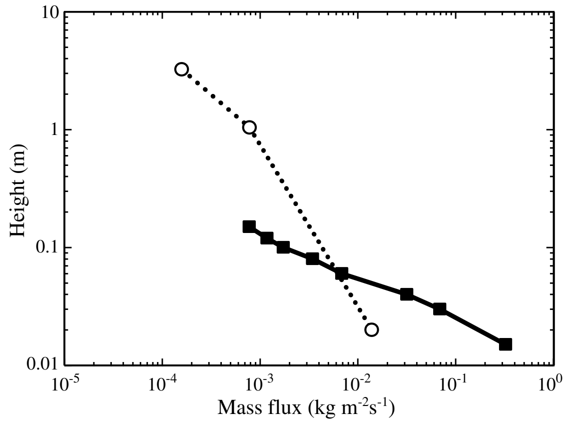

Figure 14. Horizontal snow mass flux profiles. White circle: data from field measurements (case A). Black square: data from wind tunnel experiments. Wind speed conditions are the same as those in Figure 13.

and after a certain period, these particles begin to move downward and eventually impact the surface at high speeds. These small particles moving downward at high speeds cause particles less than 100 μm in diameter (at a height of $z = 0.015$ m) to move more quickly than the wind speed, on average, although the speeds of particles moving upward as a result of particle impacts (rebound and ejection) are, in general, lower.

3.3. Comparisons Between Results of Field Measurements and Wind Tunnel Experiments

In this section, we compare the results of measurements at Col du Lac Blanc with those obtained in the wind tunnel experiments. Figure 13 shows particle diameter distributions measured at similar heights in both the field experiments and the wind tunnel. In the field experiments (case A), the friction velocity u_* was 0.35 m s^{-1} and the roughness length z_0 was 4.5×10^{-5} m, whereas in the wind tunnel experiments, u_* was 0.37 m s^{-1} and z_0 was 1.82×10^{-5} m; the values of each parameter are therefore very close to one another. Furthermore, we note that *Okaze et al.* [2012] showed that the roughness height z_0 and the friction velocity u_* estimated from an experiment with the same wind tunnel were in good agreement with the relationship between z_0 and u_* obtained in previous field research [e.g., *Tabler*, 1980].

In the field experiments, the particle size with the maximum frequency was approximately 100 μm, whereas in the wind tunnel experiments, the corresponding size was 150–250 μm. In addition, the particle size distribution in the field experiments appeared to be more skewed than that in the wind tunnel experiments, and these differences explain the discrepancy in the horizontal mass flux, as follows (see Figure 14). Near the snow surface, fluxes in the wind tunnel are approximately 1 order of magnitude greater than those observed in the field, and the fluxes also decrease more rapidly with increasing height in the field than they do in the wind tunnel. However, wind speed profiles in both cases can be regarded as approximately the same as those displayed in Figure 15, and particle speeds are in nearly equivalent ranges. Although the scales of the field measurements and the wind tunnel experiments differ, the particle speed distributions obtained in both situations under the same wind profile (as measured by the friction velocity and the surface roughness length) agree fairly well with one another.

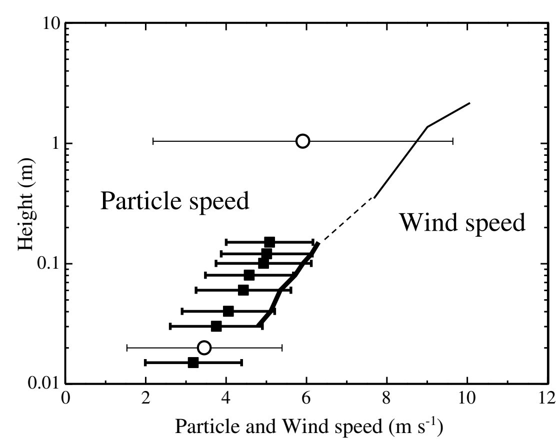

Figure 15. Particle and wind speed profiles. White circle and bold line: data from field measurements (case A). Black square and thin line: data from wind tunnel experiments. Wind speed conditions are the same as those in Figures 13 and 14. (Data points represent mean values, and the bars represent one standard deviation on either side of the mean.)

The procedures introduced in this study have been tested and are reasonably accurate, and we wish to stress that we have successfully revealed particle speeds in drifting snow conditions, as well as the dependency of particle speed on height above the snow surface, particle size, and wind speed. Furthermore, we can conclude that under the conditions of the experiments and observations, particle speeds were always 1 m s^{-1} to 2 m s^{-1} less than wind speeds at heights of 0.015–1 m. Generally, it has been believed that above the saltation layer, the thickness of which is less than 10 cm, particle

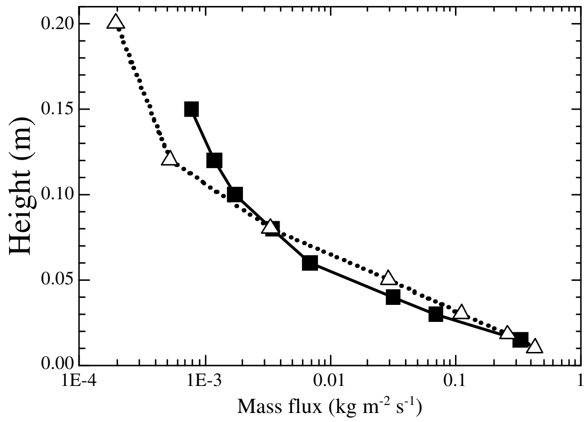

Figure 16. Horizontal mass flux profiles. White triangle: calculated flux profile for $u_* = 0.37\ \mathrm{m\ s^{-1}}$. Black square: data from wind tunnel experiments under the same conditions.

speeds are nearly the same as wind speeds. Thus, as described in section 1, the Schmidt number has usually been assumed to be unity in the model calculations [e.g., *Bintanja*, 2000; *Xiao et al.*, 2000]. However, Figure 15 reveals that momentum is still transferred from the wind to the snow particles at heights of less than 1 m at least.

4. Discussion and Conclusion

Computations of the horizontal mass flux profile shown in Figure 16 are compared with those obtained in the wind tunnel experiment for $u_* = 0.37\ \mathrm{m\ s^{-1}}$, a roughness length of 1.82×10^{-5} m, and the particle size distribution parameters α and β shown in Figure 8. The computations and the experiments are in close agreement, not only qualitatively but also quantitatively, although a slight departure of the results of the two approaches is observed at heights greater than 0.1 m. Figure 17 describes particle speeds and wind speeds calculated by the random flight model. In the calculation, wind speeds and particle speeds are nearly the same at heights greater than 0.1 m. In contrast, at heights below 0.1 m, particle speeds are less than the air speed, showing that momentum is transferred from the wind to particles in regions close to the ground. Although it is not shown in Figure 17, in a region very close to the surface (heights of less than 1 mm), particle speeds are higher than the wind speed; this is probably because particles descending into this region from above have, in general, a greater momentum than do the particles already present in this region.

However, a comparison of the simulation results with those of wind tunnel experiments conducted under the same conditions shows that the results of the two approaches do not always agree. Wind speed profiles derived from simulations and measured in wind tunnel experiments are in good agreement. Furthermore, both snow particle speeds and wind speeds increase with height, and the former are less than the latter below heights of 0.1 m, in both simulations and wind tunnel experiments. However, simulated particle speeds are always higher than measured speeds, and these differences seem to increase with height. Figure 18 shows that the simulated speeds are higher than the measured speeds for all particle sizes, except for those in the smallest size class (diameters of $< 50\ \mu$m).

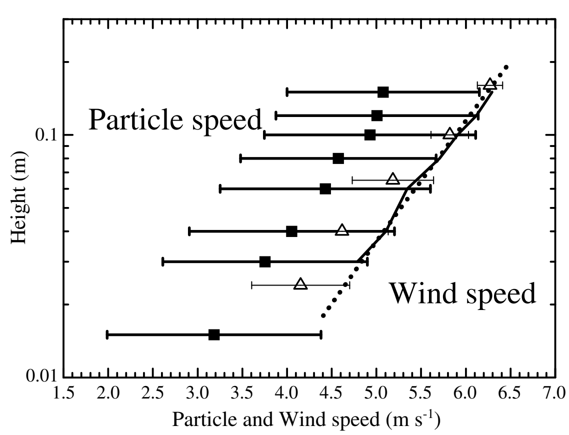

Figure 17. Particle and wind speed profiles. White triangle and solid line: calculated values. Black square and dotted line: data obtained in wind tunnel experiments. Conditions are the same as those described for Figure 16. (Data points represent mean values and the bars represent one standard deviation on either side of the mean.)

The above discrepancies suggest that the processes simulated should be examined more carefully. The fact that particle speeds differ in spite of the agreements in flux values implies that the particle size distribution may not be calculated correctly. Thus, we should reconsider the effects of turbulence, particle inertia, and processes of particle pickup from the snow surface more carefully. Furthermore, we should take into account the effects of wind tunnel length and of particle shape. As described above, several experiments were conducted at a position 6 m leeward from the wind tunnel entrance. The data obtained at this location should be compared with the data obtained at the position 12 m leeward from the entrance (see Figure 19). Obviously, both wind

10.1002/2014JD021686

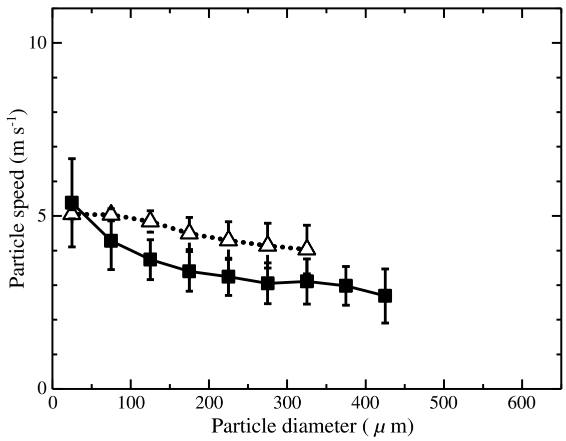

Figure 18. Snow particles speeds at $z = 0.04$ m as a function of particle diameter. White triangle: calculated values. Black square: wind tunnel experiments. Conditions are the same as those described for Figures 14 and 15. (Data points represent mean values, and the bars represent one standard deviation on either side of the mean.)

and particle speeds at 12 m are higher than those at 6 m, suggesting that drifting snow is still developing at a distance of 6 m (although *Kosugi et al*. [2005] reported that the horizontal mass flux became nearly constant at distances of greater than 2 m from the entrance). If the drifting snow is not in a steady state condition at 6 m, the particle speeds may increase or decrease at greater distances and may approach the calculated values. Furthermore, particle shapes need to be taken into account. In the calculation, the snow particles are assumed to be spherical for the determination of the drag coefficients; however, real particles are generally not spherical, as observed in Figure 8. Furthermore, only translational particle motions were taken into account in the calculations, and the effects of rotation were not considered. Thus, if the momentum transfer from the wind to the particles involves both translational and rotational transfer, and both modes are included in the model, the calculated particle speeds will decrease and the magnitudes of the differences observed in Figures 17 and 18 will be smaller. Particle–airflow–particle coupling processes need to be carefully incorporated into the calculation procedures.

Furthermore, the role of the ejection and the sweep structures in the turbulence need to be taken into account, especially the particle behavior near the bed surface, which involves aerodynamic entrainment and splash processes. *Lelouvetel et al*. [2009] conducted particle-laden flow experiments using a water channel and revealed that upward particle movement is strongly correlated to the occurrence of ejections in the vicinity of the particle. They also proposed a model of particle motion within an ejection. The detached eddy simulation was also applied to simulate particle-laden flow in an open channel by *Escauriaza and Sotiropoulos* [2011]. They took into account bed-particle interactions and the effects of instantaneous hydrodynamic forces induced by the resolved fluctuations of the coherent vertical structures. Similar approaches, as well as systematic experiments with sophisticated instruments, are required to deepen our understanding of aeolian grain transport.

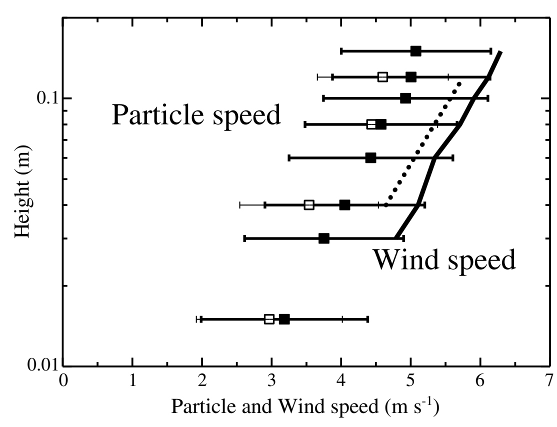

Figure 19. Particle and wind speed distributions at $u_* = 0.37\ \mathrm{m\,s^{-1}}$. White square and dotted line: data obtained at 6 m leeward from the wind tunnel entrance. Black square and solid line: data obtained at 12 m leeward from the wind tunnel entrance. (Data points represent mean values, and the bars represent one standard deviation on either side of the mean.)

Acknowledgments
The data presented in this paper are available at the Cryoscience data set, Nagoya University; please contact the authors for access to the data. The authors wish to thank all of their colleagues who participated in the field measurements and the wind tunnel experiments—the work could not have been completed without their cooperation. We are grateful to the three reviewers, who provided valuable comments and suggestions that greatly improved the quality of the manuscript. This research was supported by grants-in-aid 22253001 from the Ministry of Education, Culture, Sports, Science and Technology of Japan. This work was also supported by funding from the MAP3 ALCOTRA INTERREG, and OSUG CENACLAM programmes. Irstea is part of Labex OSUG@2020 (ANR-749 10-LABX-56).

References

Anderson, R. S., and P. K. Haff (1991), Wind modification and bed response during saltation of sand in air, *Acta Mech. Suppl.*, *1*, 21–52.
Anderson, R. S., M. Sorensen, and B. B. Willetts (1991), A review of recent progress in our understanding of Aeolian sediment transport, *Acta Mech. Suppl.*, *1*, 1–19.
Araoka, K., and N. Maeno (1981), Dynamical behaviour of snow particles in the saltation layer, *Proc. 3rd Symp. Polar Meteorol. Glaciol.*, *19*, 253–263.
Armstrong, R. L., and E. Brun (Eds.) (2010), *Snow and Climate: Physical Processes, Surface Energy Exchange and Modeling*, Cambridge Univ. Press, Cambridge.
Bagnold, R. A. (1941), *The Physics of Blown Sand and Desert Dunes*, Methuen, New York.
Bintanja, R. (2000), Snowdrift suspension and atmospheric turbulence. Part I: Theoretical background and model description, *Boundary Layer Meteorol.*, *95*, 343–368.
Bintanja, R. (2001), Characteristics of snowdrift over a bare ice surface in Antarctica, *J. Geophys. Res.*, *106*, 9653–9659, doi:10.1029/2000JD900835.
Budd, W. F. (1966), The drifting of nonuniform snow particles, in *Studies in Antarctic Meteorology*, *Antarct. Res. Ser.*, vol. 9, edited by M. J. Rubin, pp. 59–70, AGU, Washington, D. C.
Creyssels, M., P. Dupont, A. Ould El Moctar, A. Valance, I. Cantat, J. T. Jenkins, J. M. Pasini, and K. R. Rasmussen (2009), Saltating particles in a turbulent boundary layer: Experiment and theory, *J. Fluid Mech.*, *625*, 47–74.
Dery, S. J., and M. K. Yau (1999), A bulk blowing snow model, *Boundary Layer Meteorol.*, *93*, 237–251.
Doorschot, J. J. J., and M. Lehning (2002), Equilibrium saltation: Mass fluxes, aerodynamic entrainment, and dependence on grain properties, *Boundary Layer Meteorol.*, *104*(1), 111–130.
Escauriaza, C., and F. Sotiropoulos (2011), Lagrangian model of bed-load transport in turbulent junction flows, *J. Fluid Mech.*, *666*, 36–76.
Fierz, C., R. Armstrong, Y. Durand, P. Etchevers, E. Greene, D. McClung, K. Nishimura, P. Satyawali, and S. Sokratov (2009), The International Classification for Seasonal Snow on the Ground, *Tech. Rep.*, IHP-VII Technical Documents in Hydrology No. 83, IACS Contribution No. 1, UNESCO-IHP, Paris.
Gauer, P. (1998), Blowing and drifting snow in Alpine terrain: Numerical simulation and related field measurements, *Ann. Glaciol.*, *26*, 174–178.
Greeley, R., D. G. Blumberg, and S. H. Williams (1996), Field measurements of the flux and speed of wind-blown sand, *Sedimentology*, *43*, 41–52.
Hunt, J. C. R., and P. Nalpanis (1985), Saltating and suspended particles over flat and sloping surfaces, 1. Modelling concepts, in *Proceedings of the International Workshop on the Physics of Blown Sand*, edited by O. E. Barndorff-Nielsen, pp. 9–36, Univ. of Aarhus, Aarhus, Denmark.
Kind, R. J. (1992), One-dimensional aeolian suspension above beds of loose particles—A new concentration-profile equation, *Atmos. Environ.*, *26A*, 927–931.
Kosugi, K., T. Sato, N. Masaki, K. Nishimura, A. Sato, and S. Mochizuki (2005), Wind-tunnel experiments on the development of drifting snow (12)—Changes in mass flux vertical distribution at different particle diameters in drifting snow with horizontal distance [in Japanese], Preprints of the 2005 Conference Japanese Society of Snow and Ice, B4–13.
Lelouvetel, J., F. Bigillon, D. Doppler, I. Vinkovic, and J.-Y. Champagne (2009), Experimental investigation of ejections and sweeps involved in particle suspension, *Water Resour. Res.*, *45*, W02416, doi:10.1029/2007WR006520.
Liu, V., and Z. Dong (2004), Vertical profiles of aeolian sand mass flux, *Geomorphology*, *59*, 205–219.
McEwan, I. K., and B. B. Willetts (1991), Numerical model of the saltation cloud, *Acta Mech. Suppl.*, *1*, 53–66.
Morsi, S. A., and A. J. Alexander (1972), An investigation of particle trajectories in two-phase flow systems, *J. Fluid Mech.*, *55*, 193–208.
Naaim, M., F. Naaim-Bouvet, and H. Martinez (1998), Numerical simulation of drifting snow: Erosion and deposition models, *Ann. Glaciol.*, *26*, 191–196.
Nalpanis, P., J. C. R. Hunt, and C. F. Barrett (1993), Saltating particles over flat beds, *J. Fluid Mech.*, *251*, 661–685.
Nemoto, M. (2002), Dynamics of drifting snow particles in turbulent boundary-layer, PhD thesis, 98 pp., Graduate School of Environmental Earth Science, Hokkaido Univ., Japan.
Nemoto, M., and K. Nishimura (2004), Numerical simulation of drifting snow in turbulent boundary layer, *J. Geophys. Res.*, *109*, D18206, doi:10.1029/2004JD004657.
Nishimura, K., and J. C. R. Hunt (2000), Saltation and incipient suspension above a flat particle bed below a turbulent boundary layer, *J. Fluid Mech.*, *417*, 77–102.
Nishimura, K., and M. Nemoto (2005), Blowing snow at Mizuho station, *Antarctica. Philos. T. Roy. Soc. A*, *363*, 1647–1662.
Okaze, T., A. Mochida, Y. Tominaga, M. Nemoto, T. Sato, Y. Sasaki, and K. Ichinohe (2012), Wind tunnel investigation of drifting snow development in a boundary layer, *J. Wind Eng. Ind. Aerodyn.*, *104–106*, 532–539.
Rasmussen, K. R., and H. E. Mikkelsen (1998), On the efficiency of vertical array aeolian field traps, *Sedimentology*, *45*, 789–800.
Rasmussen, K. R., and M. Sorensen (2005), Dynamics of particles, in *Aeolian Saltation: Powder and Grains*, edited by R. Garcia-Rojo, H. J. Herrmann, and S. McNamara, pp. 967–971, A. A. Balkema, Brookfield, Vt.
Sato, T., T. Kimura, T. Ishimaru, and T. Maruyama (1993), Field test of a new snow-particle counter (SPC) system, *Ann. Glaciol.*, *18*, 149–154.
Sato, T., K. Kosugi, and A. Sato (2001), Saltation-layer structure of drifting snow observed in a wind tunnel, *Ann. Glaciol.*, *32*, 203–208.
Schmidt, R. A. (1977), A system that measures blowing snow, USDA Forest Service Research Paper, RM-194, 80 pp., Rocky Mountain Forest and Range Experiment Station, Fort Collins, Colo.
Schmidt, R. A. (1982), Vertical profiles of wind speed, snow concentration, and humidity in blowing snow, *Boundary Layer Meteorol.*, *23*, 223–246.
Shao, Y., and A. Li (1999), Numerical modelling of saltation in the atmospheric surface layer, *Boundary Layer Meteorol.*, *91*, 199–225.
Sugiura, K., and N. Maeno (2000), Wind-tunnel measurements of restitution coefficients and ejection number of snow particles in drifting snow: Determination of splash functions, *Boundary Layer Meteorol.*, *95*, 123–143.
Tabler, R. D. (1980), Self-similarity of wind profiles in blowing snow allows outdoor modelling, *J. Glaciol.*, *26*(94), 421–434.
Takeuchi, M. (1980), Vertical profile and horizontal increase of drift-snow transport, *J. Glaciol.*, *26*(94), 481–492.
Tong, D., and N. Huang (2012), Numerical simulation of saltating particles in atmospheric boundary layer over flat bed and sand ripples, *J. Geophys. Res.*, *117*, D16205, doi:10.1029/2011JD017424.
Uematsu, T. (1993), Numerical study on snow transport and drift formation, *Ann. Glaciol.*, *18*, 135–141.
Unger, J., and P. K. Haff (1987), Steady state saltation in air, *Sedimentology*, *34*, 289–299.
White, B. R., and H. Mounla (1991), An experimental study of Froude number effect on wind-tunnel saltation, *Acta Mech. Suppl.*, *1*, 145–157.
Willetts, B. B., and M. A. Rice (1985), Intersaltation collisions, in *Proceedings of the International Workshop on the Physics of Blown Sand*, edited by O. E. Barndorff-Nielse, pp. 89–100, Univ. of Aarhus, Denmark.
Wilson, J. D., and B. L. Sawford (1996), Review of Lagrangian stochastic models for trajectories in the turbulent atmosphere, *Boundary Layer Meteorol.*, *97*, 109–135.
Xiao, J., R. Bintanja, S. J. Dery, G. W. Mann, and P. A. Taylor (2000), An intercomparison among four models of blowing snow, *Boundary Layer Meteorol.*, *97*, 191–210.
Yang, P., Z. Dong, G. Qian, W. Luo, and H. Wang (2007), Height profile of the mean velocity of an aeolian saltating cloud: Wind tunnel measurements by particle image velocimetry, *Geomorphology*, *89*, 320–334.

